ORIGINAL ARTICLE

Crucial role for lung iron level and regulation in the pathogenesis and severity of asthma

Md Khadem Ali[1,2], Richard Y. Kim[2,3], Alexandra C. Brown[2], Jemma R. Mayall[2], Rafia Karim[2], James W. Pinkerton[2,4], Gang Liu[2,3], Kristy L. Martin[5], Malcolm R. Starkey[2,6], Amber Pillar[2], Chantal Donovan[2,3], Prabuddha S. Pathinayake[7], Olivia R. Carroll[2], Debbie Trinder[8], Hock L. Tay[2], Yusef E. Badi[9], Nazanin Z. Kermani[10], Yi-Ke Guo[10], Ritambhara Aryal[5], Sharon Mumby[9], Stelios Pavlidis[9], Ian M. Adcock[9], Jessica Weaver[2], Dikaia Xenaki[11], Brian G. Oliver[11], Elizabeth G. Holliday[12], Paul S. Foster[2], Peter A. Wark[2,13], Daniel M. Johnstone[14], Elizabeth A. Milward[5], Philip M. Hansbro[2,3,#] and Jay C. Horvat[2#]

Affiliations: [1]Division of Pulmonary and Critical Care Medicine, Stanford University, California, United States of America. [2]Priority Research Centre for Healthy Lungs, Hunter Medical Research Institute and School of Biomedical Sciences and Pharmacy, University of Newcastle, Newcastle, New South Wales, Australia. [3]Centre for Inflammation, Centenary Institute, and Faculty of Science, University of Technology Sydney, Sydney, New South Wales, Australia. [4]Respiratory Pharmacology & Toxicology Group, National Heart & Lung Institute, Imperial College London, London, United Kingdom. [5]School of Biomedical Sciences and Pharmacy, The University of Newcastle, Newcastle, New South Wales, Australia. [6]Department of Immunology and Pathology, Central Clinical School, Monash University, Melbourne, Victoria, Australia. [7]Priority Research Centre for Healthy Lungs, Hunter Medical

Research Institute and School of Medicine and Public Health, University of Newcastle, Newcastle, New South Wales, Australia. [8]Medical School, Harry Perkins Medical Research Institute, University of Western Australia, Fiona Stanley Hospital, Perth, Western Australia, Australia. [9]Airway Disease Section, National Heart & Lung Institute, Imperial College London, London, United Kingdom. [10]Data science institute, Department of computing, Imperial College London. [11]Woolcock Institute of Medical Research, University of Sydney and School of Life Sciences, University of Technology Sydney, Sydney, NSW, Australia. [12]Hunter Medical Research Institute, New Lambton, New South Wales, Australia and School of Medicine and Public Health, University of Newcastle, Callaghan, New South Wales, Australia. [13]Department of Respiratory and Sleep Medicine, John Hunter Hospital, Newcastle, New South Wales, Australia. [14]Discipline of Physiology and Bosch Institute, University of Sydney, Sydney, New South Wales, Australia.

[#]Authors contributed equally

*Correspondence and requests for reprints should be addressed to Associate Professor Jay Horvat, PhD, Priority Research Centre for Healthy Lungs, Hunter Medical Research Institute, Lot 1 Kookaburra Circuit, New Lambton Heights, Newcastle, New South Wales, 2305, Australia. Email: jay.horvat@newcastle.edu.au

Online Repository

Supplementary Methods

Study approvals

All experiments were conducted with approval of the Human/Animal Research Ethics Committees of the University of Newcastle, Australia and the Unbiased Biomarkers in Prediction of respiratory disease outcomes (U-BIOPRED) centre.

Human subjects

Airway biopsy tissues and bronchoalveolar lavage (BAL) were collected from 11 severe, 12 mild-moderate asthmatics and 13 healthy subjects. To measure non-haem iron content in BAL supernatant, BAL samples were also collected from a second set of severe or mild-moderate asthma patients and healthy subjects (10 subjects in each group). Subjects with severe or mild-moderate asthma had mean FEV1% predicted at 86.92 ± 2.726 ($p0.01$) and 76 ± 5.389 ($p0.001$), respectively, compared to healthy controls (102.7 ± 4.494, **Table 1**). BAL was collected from another set of 10 subjects in each group: severe (mean FEV1% predicted, 66.33 ± 7.427, $p<0.01$) or mild-moderate asthma (mean FEV1%, 89.6 ± 4.759) or healthy controls (mean FEV1%, 97.5 ± 5.861) (**Table 2**). Human bronchial airway epithelial cells (pBECs), airway smooth muscle (ASM) cells and lung fibroblasts donor characteristics are shown in **Tables E5 and 6**. Patient exclusion criteria included current smokers, recent exacerbation, respiratory tract infection in the last 4 weeks and age younger than 18yrs.

Human BAL

For each donor, BAL was collected by instilling sterile warm saline (2x 60mL) into the airways using elective fibreoptic bronchoscopy, as described previously (1). Collected BAL was

filtered through a nylon filter apparatus, centrifuged (400x g, 10 mins) and then supernatant was stored at $-80°C$ for future analysis. BAL cell pellets were resuspended in PBS and cytospins were prepared, stained with Diff-quik solutions for 30 sec, solution II (fixative) for 30 sec, solution I for 30 sec, dehydrated and air-dried overnight for cover slipping. Differential cells were analysed based on morphology as previously described (1).

Quantification of iron-laden BAL cells

Total iron positive cells and iron score index levels were calculated by enumerating the different grade of iron scored cells (Grade 0, 1, 2 and 3) using Perls'-DAB stained (*see below*) BAL cytospins.

Mouse models of iron overload

We utilised two models of iron overload to assess the effects of iron on asthma. We first used female $Hfe^{-/-}$ and WT mice (36 weeks old) (2) on an AKR background strain that were fed a normal diet. Disruption of this gene results in deficiency in hepcidin production, leading to increased systemic iron levels (2-4). In addition, female BALB/c mice (6-8 weeks of age) were fed a diet of mouse chow that contains 2% carbonyl iron (19410mg Fe/Kg diet, Specialty Feeds, Western Australia) *ad libitum* for 8 weeks. This results in a similar level of iron load in the liver as $Hfe^{-/-}$ mice. WT BALB/c mice were also maintained on control iron diet (~49 mg Fe/Kg diet) or low iron diet (~2.5mg Fe/Kg diet, Speciality Feeds, Western Australia) for 8 weeks as a comparison. All mice were housed at $22 \pm 2°$ temperature with humidity range of 30-70 under 12 hours dark/light cycling conditions.

HDM-induced chronic experimental asthma

WT AKR and *Hfe*$^{-/-}$ female mice (~36 weeks old), and WT BALB/c female mice (8 weeks old) fed low iron, control and high iron diets were intranasally administered HDM extract (25µg, 50 µl PBS, Greer Laboratories, Lenoir, NC) or vehicle (PBS) 5 days per week for 6 weeks. After 6 weeks, liver and lung tissues were collected for further analysis, and AHR was measured.

Perls' and DAB-enhanced Perls' stain

The single lobed lungs from mice were perfused with saline, inflated and fixed with formalin, paraffin-embedded, and sectioned (4-6µm). Sections were deparaffinised with xylene and a graded series of ethanol. Deparaffinised mouse lung sections or BAL cell cytospins prepared from clinical and experimental samples were submerged in fresh 1% Potassium Ferrocyanide (AnalaR), pH 1 (Perls' solution), for 30 min on a shaker. Each slide was washed briefly in distilled water, incubated in methanol containing 0.01M NaN$_3$ (MERCK) and 0.3% H$_2$O$_2$ for 1 h on a shaker. Slides were rinsed in 0.1M PBS (pH7.4) and iron staining was enhanced by 1 h of incubation with 0.025% 3, 3'-Diaminobenzidine-4HCl (DAB, MP Biomedical) and 0.005% H$_2$O$_2$ in 0.1M PBS (pH 7.4) on a shaker. Slides were then washed in distilled water, dehydrated with a series of graded ethanol, cleared with xylene, and cover slipped using DEPEX mounting medium (BDH Chemical).

Non-haem iron assay for the assessment of iron levels in BAL supernatants and tissue

Non-haem iron content in BAL supernatants from severe or mild-moderate asthma patients or healthy controls, and in murine liver and lung tissues were measured as previously described (5). For the latter, briefly, ~50mg of wet tissues of liver or lung were homogenised in 1 ml of 0.9% NaCl solution on ice. Iron standard solutions ranging in concentration from 0 to 8µg/ml

were prepared from a stock solution of 5mM $FeSO_4$ (BDH Chemical). Then 100µl of iron standards or BAL supernatant or tissue homogenates were mixed with 50µL of 3.8M (12%) HCl and incubated at 85°C for 30 min. Then, 25µL of 50% trichloroacetic acid (Sigma-Aldrich, Australia) was added into each tube followed by incubated on ice for 10 min. After centrifugation (235 xg, room temperature, 20 min), 100 µl of supernatant was removed from each tube and added in triplicate to clear 96-well plates. Finally, 100µl of colour reagent (816µM bathophenanthroline disulfonic acid, 1.9M sodium acetate, 0.2% (v/v) thioglycolic acid; Sigma) was added to each well to develop colour and absorbance was measured at 560nm using a microplate reader (Synergy2, Millennium Science). After subtracting absorbance of blank samples, iron concentrations were calculated from the standard curve.

Gene expression analysis by RT-qPCR

Total RNA was extracted from frozen mouse lung tissues using Trizol reagent (Invitrogen, Life Technologies, Australia) as described previously (6). Mouse total RNA (1µg) was reverse transcribed into cDNA using Bioscript (Bioline, Australia) and random hexamer primers (Invitrogen, Life Technologies, Australia). For human airway biopsy tissues, total RNA was isolated using QIAGEN RNeasy Mini kit for human airway biopsy tissue homogenates (Qiagen, Venlo, Netherlands, Cat# 990394) according to the manufacturer's instructions. Human cDNA was collected using a reverse transcription kit (Applied Biosystems, USA). The level of mRNA transcripts for iron regulatory molecules and cytokines were measured by SYBR-green qPCR using Eppendorf RealPlex (Eppendorf, Germany) and relative expression was normalised to transcripts of *HPRT* (mouse gene expression) or beta actin (human gene expression) (7-9). The formula used for calculating relative expression of each gene of interest was $2^{-(Ct\ gene\ of\ interest\ -\ Ct\ HPRT)}$ (10). Primer sequences are shown in **Tables E1 and 2**. Total mRNA from primary human ASM cells and lung fibroblast culture experiments was isolated using the

ISOLATE II RNA Mini Kit and transcribed into cDNA using the SensiFAST™ cDNA Synthesis Kit (Bioline, Alexandria, Australia), according to the manufacturer's instructions. Assays were carried out in triplicate using a reaction mixture containing the Bioline SensiFAST Probe Hi-ROX Master Mix and TaqMan primer sets for *TNC* (Hs01115665_m1) and the ubiquitously expressed ribosomal RNA (18S rRNA) as a housekeeping gene. qPCR was performed using the StepOnePlus detection system and data were collected and analysed by StepOne software (Applied Biosystems, Melbourne, Australia).

Mouse BAL

BAL collection, processing and cytospin preparations were performed as described previously (11). BAL cells cytospin slides were stained with May-Grunwald-Giemsa, differential immune cells were counted (≈175) using light microscopy at 40x magnification based on key morphological characteristics (12, 13).

Lung tissue eosinophil and airway mucus-secreting cell numbers

Lung sections were deparaffinised and stained with chrome salt fixation (for eosinophils) or periodic acid–Schiff (for mucus-secreting cells). Numbers of eosinophils and PAS positive cells (i.e. mucus secreting cells) were counted per 100µm around the airways at 100x magnification as previously described (12, 13).

Small airway remodelling

Airway remodelling in terms of collagen thickness around the small airways was evaluated in at least 6 small airway images (40x magnification) from Sirius Red and Fast Green-stained (Sigma Aldrich, USA) mouse lung sections using ImageJ (version 1.47, Media Cybernetics, Rockville, MD, USA) as previously described (11).

AHR

AHR in terms of central airway resistance (Rn) in response to nebulised methacholine (MCh) was measured using FlexiVent apparatus (FX1 System; SCIREQ, Montreal, Canada). Briefly, mice were anaesthetised with a mixture of ketamine (100mg/kg, Parnell)) and xylazine (10mg/kg, Troy Laboratories, Smithfield, Australia). Following tracheostomy, cannulae were inserted into their tracheas and ligated (7, 12-14). Rn (tidal volume of 8mL/kg at a respiratory rate of 450 breaths/min) was measured in response to increasing doses of nebulised MCh (up to 30mg/kg; Sigma-Aldrich, Sydney, Australia) (14).

IL6, IL8 and transferrin detection. Levels of IL-6 and IL-8 in cell-free supernatants were measured by sandwich ELISA, using commercial antibody kits according to the manufacturer's instructions (R&D Systems, MN). The detection limit of both assays was 15.6 pg/ml. Levels of transferrin in BAL supernatants were measured using commercial ELISA kit according to the manufacturer's instructions (Abcam: ab157724).

Flow cytometric analysis of macrophage populations in murine lung tissue.

Flow cytometry was performed on murine whole lung single cell suspensions to determine the number and activation of macrophage subsets (15). Lung tissue was processed into single cell suspensions *via* enzymatic digestion with collagenase D (2mg/mL, Roche, Sydney, Australia), DNase I (400U/mL, Roche) and a gentleMACS™ Dissociator (Miltenyi Biotec). Total lungs cells were collected, and red blood cells lysed (155mM NH4Cl, 12mM NaHCO3, 0.1mM ethylenediaminetetraacetic acid [EDTA], pH 7.35, 5mins, 4°C). Total cell counts were performed using a haemocytometer under a light microscope (20x magnification) and trypan blue (Sigma-Aldrich) exclusion. Total cells stained with fluorescently conjugated antibodies

specific for CD45, F4/80, CD11c, CD11b, Ly6C, SiglecF and TFR1 (**Table E3**) (BD Biosciences, San Diego, USA; Biolegend, San Diego, USA). Live cell discrimination was assessed with Zombie yellow fixable viability dye (Biolegend). Cells were then analysed using a LSR Fortessa X-20 (BD Biosciences) and FACSDiva software (BD Biosciences). After exclusion of cell debris, doublets and dead cells, macrophage subsets were determined based on antigen expression (**Table E4**).

Isolation of macrophages from whole lung tissue. Lungs were processed into single cell suspensions and stained with fluorochrome-conjugated antibodies as above. $Tfr1^+$ macrophages were isolated by fluorescence-activated cell sorting using an ARIA III (BD Biosciences) into PBS with 5% FCS.

RNA extraction from isolated macrophages and reverse transcription (RT).

Total RNA was extracted from sorted $Tfr1^+$ macrophages using miRNeasy mini kit (Qiagen, Chadstone, Australia) as per manufacturer's instructions. Sorted cells were collected into Qiazol® (750μL) and stored at -80^oC until RNA extraction. Upon thawing of cells, chloroform (140 μL) was added and vortexed prior to phase separation by centrifugation (15min, 4˚C, 12,000xg). The aqueous phase was collected before automated RNA extraction using Qiacube apparatus (Qiagen). This automated protocol supplemented samples with 100% molecular grade ethanol prior to centrifugation. Samples were transferred to spin columns and washed with RWT buffer. RPE buffer was added to columns prior to further centrifugation. Purified RNA was eluted using RNAse-free water. RNA purity and concentration were determined using a NanoDrop™ 1000 Spectrophotometer (Thermo Fisher Scientific, North Ryde, Australia). The 260/230nm and 260/280nm absorption ratios accepted as pure RNA was >1.90, and >2.00, respectively. RNA from isolated macrophages was reverse transcribed to cDNA

using the miScript II RT kit (Qiagen) as per manufacturer's instructions. Samples were supplemented with miScript HiFlex buffer (4µl), 10x miScript Nucleics mix (2µl) and miScript reverse transcriptase mix (2µl). Reverse transcription was achieved using a Bio-Rad T100 Thermal Cycler (60min, 37ºC; 5min, 95ºC). Samples were then stored at -20ºC until quantification by qPCR.

ASM cell and lung fibroblasts culture. Primary human ASM cells and lung fibroblasts were isolated from the parenchyma of lungs from patients undergoing lung transplantation as previously described (16). Patient demographics are described in **Table E6**. Cells were seeded in 12 or 96 well plates at $4.5{\times}10^4$ cells/mL in DMEM with 5% fetal bovine serum and 1% antibiotic-antimycotic, and cultured to near confluence (72h, 37°C, 5% CO_2). Cells were serum starved in DMEM with 0.1% bovine serum albumin for 24h prior to stimulation. Cells were stimulated with a range of ferric ammonium citrate (FAC) concentrations for 48h, with additions replenished at 24h. Cell free supernatants or total RNA lysates were collected at 48h and stored at -20°C for analysis. All experiments were carried out using fibroblasts between passage 2 and 4.

Primary bronchial airway epithelial cells (pBECs) cultured at the air-liquid interface (ALI) (17). Human pBECs were obtained from healthy controls, and patients with severe asthma. pBECs were raised and maintained in placental collagen-coated T75 tissue culture flasks (Interpath, Australia) with Bronchial Epithelial Cell Growth Medium (BEGM™, Lonza, USA), supplemented with BEGM™ SingleQuots™ supplements and Growth Factors (BEGM™ BulletKit™, Lonza), penicillin/streptomycin (Life Technologies, USA) and amphotericin B (Sigma, USA). Cell monolayers at 70%-80% confluency were detached with 1:10 trypsin-ethylenediaminetetraacetic acid/Dulbecco's phosphate buffered saline (1:10

trypsin-EDTA/D-PBS, 4mL). Trypsin enzyme activity was neutralised with foetal bovine serum (FBS) and cells were resuspended in ALI initial medium. Detached cells were then enumerated and seeded at $2x10^5$ cells/500µL initial media onto the apical compartment of a 12-well plate (Corning, USA) containing a 12mm polyester membrane transwell (0.4µm pore size, Sigma). ALI initial media was also added to the basal compartment (1.5mL/well) and refreshed (1.5mL/well) 24h after seeding. At 72h post-seeding, all apical media was removed and basal media replaced with ALI final medium (1.5mL/well). This timepoint was demarcated as "day 0" of ALI culture and the beginning of the experimental period. Basolateral media was replaced every two days with 1.5mL fresh ALI final medium. Apical surfaces of the ALI cultures were washed with sterile 1xD-PBS (500uL/well) weekly, and trans-epithelial electrical resistance measured (Epithelial Volt/ohmmeter 2 [EVOM$_2$], Coherent Scientific) to track monolayer formation. This weekly apical wash also served to remove any mucus build-up from the cultures. Patient cells were grown at ALI in culture conditions (37°C, 5% CO_2) for 28 days to ensure maximal differentiation. Following sufficient differentiation of the cells basal media was replaced with ALI minimal media (1.5 mL/well) and incubated overnight (37°C, 5% CO_2). Apical compartments of each well were then supplemented with minimal media and 1xD-PBS (500uL) and basal minimal media was replaced (1.5mL) prior to the second overnight incubation (37°C, 5% CO_2). At the end of the protocol, apical and basal media was removed and stored at -80°C for further analysis. Cells from the apical ALI membrane insert were also harvested and stored in Qiazol® lysis reagent (700uL, Qiagen, -80°C) for further processing.

Statistics

Comparisons between two groups were performed using a non-parametric Mann-Whitney test. Comparisons between multiple groups were performed using Kruskal-Wallis one-way analysis of variance (ANOVA) with uncorrected Dunn's post-hoc test. AHR data were analysed using

two-way repeated measures ANOVA with Bonferroni post-hoc test. Correlation analyses were performed using Spearman rank correlation. All statistical analysis was performed using GraphPad Prism V.7 Software (San Diego, California, USA).

Supplementary results

HDM-induced experimental asthma

Intranasal HDM-treatment increases the number of immune cells (macrophages, neutrophils, eosinophils) in BAL, airway tissue eosinophil numbers, mucus secreting cell numbers, and collagen deposition in airway tissue and this is associated with increased airway hyper-responsiveness (AHR) (**Figure E2 A-F**).

Supplementary discussion

We show a significant increase in iron positive BAL cells in subjects with severe and mild-moderate asthma compared to healthy controls. Increased numbers of iron-laden cells have been reported in patients with COPD (18), IPF (19) and cigarette smokers (20). The increased iron in the lung of cigarette smokers may not be dyshomeostasis, but actual loading of lungs with additional iron on inhalation. However, these findings do suggest that increased numbers of iron laden cells in the airways is a key feature of several lung diseases. Our data is also consistent, with a recent case report where haemosiderin-laden macrophages were identified in BAL from an 8-year old child with recurrent iron-deficiency anaemia (IDA) and allergic asthma and later diagnosed with idiopathic pulmonary haemosiderosis (IPH) (21). However,

since this study is based on a single patient it is unclear whether IDA and/or macrophage haemosiderin are associated with allergic asthma or IPH.

To protect from the potentially harmful effects of excess free iron, iron regulatory systems must be tightly regulated in the body. Although little is known about the iron metabolism in the lung, as with other organs, iron homeostasis in the lung is maintained by a range of iron regulatory molecules, including iron uptake (transferrin receptors, TFR1, TFR2); divalent metal transporter 1 (DMT1); zinc transporter protein 14 (ZIP14); natural resistance-associated macrophage protein 1 (NRAMP1) and lactoferrin receptor (LFR); transport (Transferrin, TF), storage (ferritin heavy and light chain, FTH, FTL) and export (ferroportin, FPN) from cells. Iron-responsive proteins (IRPs) control the expression of these genes through binding with the 5′ or 3′ untranslated regions of these genes mRNA (22).

We show that *NRAMP1* expression is higher in the airways of mild-moderate asthma patients and tends to further increase in severe asthma compared to healthy controls (**Figure 3C**). NRAMP1 has been reported to affect IgE responses, the development of Th2 cell responses and mast cell degranulation in ovalbumin-induced allergic asthma in mice (23). We also show increased *TFR2* in the airways of severe asthma patients (**Figure 3A**). TFR2 acts as an iron sensor of transferrin-bound iron (Fe-TF) that stimulates hepcidin production (24). In addition, ZIP14 levels have been shown to increase in airway cells in iron overload and decrease in iron deficiency in mice (25). We show increased *FTH* and *IRP1* expression in airways of mild-moderate but not severe asthma patients (**Figure 3D, F**). Furthermore, *FTL* expression reduced ($p=0.06$) in the airways of severe compared to mild-moderate asthma patients (**Figure 3E**). Another study suggested that *FTL* has anti-inflammatory effects, which agree with our findings (26). In addition, we find that the only known iron exporter, *FPN* expression is not altered in asthma (**Figure 3H**). All these data provide strong evidence that

there is an environment of increased iron sequestration into cells in asthmatic airways that leads to increased cellular but reduced extracellular iron levels in BAL in asthma.

To explore the relationship between iron and asthma, we performed a series of studies to determine the effects of LID on key disease features. Decreasing systemic iron levels using a LID had no effect on lung iron levels but increased AHR in the absence of HDM-induced experimental asthma. However, we also show that a LID reduces iron accumulation in HDM-induced experimental asthma and protects against some of the key features of disease. These findings highlight the complexity and importance of systemic:local iron regulatory interactions in the pathogenesis of asthma, and also demonstrates that both low and high systemic iron may promote/increase the severity of key disease features in different contexts, which is consistent with the controversy in the literature (27-32).

Whilst our findings demonstrate that increased iron accumulation in cells and tissues in the airways and lung is linked to key features of asthma and plays a role in the worsening of lung function and disease severity, they do not elucidate the underlying mechanisms involved in iron-mediated effects. A large body of evidence suggests that iron-induced oxidative stress may play a key role (24). Iron accumulation has been suggested to induce oxidative stress and contribute to the pathogenesis of Alzheimer's disease, atherosclerosis and Parkinson's disease (33), and there is a clear involvement of oxidative stress in asthma (34, 35). Increased production of ROS and reactive nitrogen species (RNS) and reduced or inactivated antioxidant responses occur in patients with bronchial asthma (36-40). Lipid peroxidation in plasma and exhaled breath condensate (EBC) is inversely correlated with airflow obstruction in asthma (41). In addition, total antioxidant capacity in plasma and sputum, and SOD levels in plasma and airway epithelial cells (AEC) have been reported to be positively associated with airflow obstruction in asthmatics (41). Chronic inflammation can generate ROS (42), and overproduction of ROS/RNS reportedly leads to airway inflammation and remodelling, mucus

overproduction, tissue injury and lung function decline in clinical and experimental asthma studies (43, 44). Notably, a significant increase in iron and MDA levels in plasma have been shown in asthmatics, and there is a positive correlation between MDA and iron levels (32), suggesting that increased systemic iron may promote asthma. Furthermore, increased levels of oxidative stress (increased MDA, catalase, SOD, GPX and nitrotyrosine levels) and inflammatory responses (increased HIF1α, NF-κB and TNFα levels) with increased iron accumulation in the lung have been shown in rats treated with low molecular weight iron dextran (45). Based on this evidence, increased iron may drive disease through increased oxidative stress in tissues that drives many of the key features of disease.

Ferroptosis, a process of iron-dependent programmed cell death, has recently been suggested to be a key molecular mechanisms implicated in kidney, brain, liver, heart and lung pathology (46-51). Recently, Wenzel *et al.*, uncovered evidence for phosphatidylethanolamine-binding protein 1 (PEBP1)-dependent regulatory mechanisms of ferroptotic death in AEC in asthma (52). Since we show that experimental asthma results in increased iron accumulation in lung cells and tissues as well as evidence for increased iron sequestration in clinical airway samples, it is possible that increased iron accumulation-mediated ferroptotic cell death may contribute to disease pathogenesis. However, further studies are required to explore mechanisms of the association between iron and ferroptosis in asthma pathogenesis and to determine the $Fe^{2+/3+}$ status and localisation within airway cells.

In the lung, iron can also be derived from non-dietary sources e.g smoking, pollution or geogenic iron. Increased iron accumulation in the lung as a result of these exogenous exposures may also contribute to lung pathology. Indeed, Indeed, a recent study has shown that increased concentrations of iron in particulate matter result in lung impairment 7 days-post intranasal exposure in mice (53). It is also important to note that infections are associated with the development of asthma phenotypes and that humans and mice with asthma or allergic

airway disease have altered microbiomes and predispose to respiratory infections that increase the severity or exacerbate their disease (24) . Excess iron can also increase susceptibility to respiratory infections (24), which may modify the immune system and promote disease pathogenesis.

Due to the limited availability of appropriate airway tissue samples, and the prospective nature of our analyses, we needed to draw bronchoscopy samples from two different cohorts. We note that there was no significant difference in asthma control questionnaire (ACQ) and BAL cellular profiles in the cohorts that we used for BAL non-haem iron studies. Our findings from these two different cohorts highlight that iron levels and regulation are altered in asthma.

References

1. Vlahos R, Wark PA, Anderson GP, Bozinovski S. Glucocorticosteroids differentially regulate MMP-9 and neutrophil elastase in COPD. *PLoS One* 2012; 7: e33277.

2. Zhou XY, Tomatsu S, Fleming RE, Parkkila S, Waheed A, Jiang J, Fei Y, Brunt EM, Ruddy DA, Prass CE, Schatzman RC, O'Neill R, Britton RS, Bacon BR, Sly WS. HFE gene knockout produces mouse model of hereditary hemochromatosis. *Proc Natl Acad Sci U S A* 1998; 95: 2492-2497.

3. Gao J, Chen J, De Domenico I, Koeller DM, Harding CO, Fleming RE, Koeberl DD, Enns CA. Hepatocyte-targeted HFE and TFR2 control hepcidin expression in mice. *Blood* 2010; 115: 3374-3381.

4. Schmidt PJ, Toran PT, Giannetti AM, Bjorkman PJ, Andrews NC. The transferrin receptor modulates Hfe-dependent regulation of hepcidin expression. *Cell Metab* 2008; 7: 205-214.

5. Kaldor I. Studies on intermediary iron metabolism. V. The measurement of non-haemoglobin tissue iron. *Aust J Exp Biol Med Sci* 1954; 32: 795-799.

6. Collison A, Hatchwell L, Verrills N, Wark PA, de Siqueira AP, Tooze M, Carpenter H, Don AS, Morris JC, Zimmermann N, Bartlett NW, Rothenberg ME, Johnston SL, Foster PS, Mattes J. The E3 ubiquitin ligase midline 1 promotes allergen and rhinovirus-induced asthma by inhibiting protein phosphatase 2A activity. *Nat Med* 2013; 19: 232-237.

7. Beckett EL, Stevens RL, Jarnicki AG, Kim RY, Hanish I, Hansbro NG, Deane A, Keely S, Horvat JC, Yang M, Oliver BG, van Rooijen N, Inman MD, Adachi R, Soberman RJ, Hamadi S, Wark PA, Foster PS, Hansbro PM. A new short-term mouse model of chronic obstructive pulmonary disease identifies a role for mast cell tryptase in pathogenesis. *J Allergy Clin Immunol* 2013; 131: 752-762.

8. Essilfie AT, Horvat JC, Kim RY, Mayall JR, Pinkerton JW, Beckett EL, Starkey MR, Simpson JL, Foster PS, Gibson PG, Hansbro PM. Macrolide therapy suppresses key features of experimental steroid-sensitive and steroid-insensitive asthma. *Thorax* 2015; 70: 458-467.

9. Asquith KL, Horvat JC, Kaiko GE, Carey AJ, Beagley KW, Hansbro PM, Foster PS. Interleukin-13 promotes susceptibility to chlamydial infection of the respiratory and genital tracts. *PLoS Pathog* 2011; 7: e1001339.

10. Horvat JC, Starkey MR, Kim RY, Phipps S, Gibson PG, Beagley KW, Foster PS, Hansbro PM. Early-life chlamydial lung infection enhances allergic airways disease through age-dependent differences in immunopathology. *J Allergy Clin Immunol* 2010; 125: 617-625, 625 e611-625 e616.

11. Liu G, Cooley MA, Jarnicki AG, Hsu AC, Nair PM, Haw TJ, Fricker M, Gellatly SL, Kim RY, Inman MD, Tjin G, Wark PA, Walker MM, Horvat JC, Oliver BG, Argraves WS,

Knight DA, Burgess JK, Hansbro PM. Fibulin-1 regulates the pathogenesis of tissue remodeling in respiratory diseases. *JCI Insight* 2016; 1.

12. Horvat JC, Beagley KW, Wade MA, Preston JA, Hansbro NG, Hickey DK, Kaiko GE, Gibson PG, Foster PS, Hansbro PM. Neonatal chlamydial infection induces mixed T-cell responses that drive allergic airway disease. *Am J Respir Crit Care Med* 2007; 176: 556-564.

13. Horvat JC, Starkey MR, Kim RY, Beagley KW, Preston JA, Gibson PG, Foster PS, Hansbro PM. Chlamydial respiratory infection during allergen sensitization drives neutrophilic allergic airways disease. *J Immunol* 2010; 184: 4159-4169.

14. Kim RY, Horvat JC, Pinkerton JW, Starkey MR, Essilfie AT, Mayall JR, Nair PM, Hansbro NG, Jones B, Haw TJ, Sunkara KP, Nguyen TH, Jarnicki AG, Keely S, Mattes J, Adcock IM, Foster PS, Hansbro PM. MicroRNA-21 drives severe, steroid-insensitive experimental asthma by amplifying phosphoinositide 3-kinase-mediated suppression of histone deacetylase 2. *J Allergy Clin Immunol* 2017; 139: 519-532.

15. Starkey MR, Nguyen DH, Brown AC, Essilfie AT, Kim RY, Yagita H, Horvat JC, Hansbro PM. Programmed Death Ligand 1 Promotes Early-Life Chlamydia Respiratory Infection-Induced Severe Allergic Airway Disease. *Am J Respir Cell Mol Biol* 2016; 54: 493-503.

16. Krimmer D, Ichimaru Y, Burgess J, Black J, Oliver B. Exposure to biomass smoke extract enhances fibronectin release from fibroblasts. *PLoS One* 2013; 8: e83938.

17. Hsu AC, Starkey MR, Hanish I, Parsons K, Haw TJ, Howland LJ, Barr I, Mahony JB, Foster PS, Knight DA, Wark PA, Hansbro PM. Targeting PI3K-p110alpha Suppresses Influenza Virus Infection in Chronic Obstructive Pulmonary Disease. *Am J Respir Crit Care Med* 2015; 191: 1012-1023.

18. Philippot Q, Deslee G, Adair-Kirk TL, Woods JC, Byers D, Conradi S, Dury S, Perotin JM, Lebargy F, Cassan C, Le Naour R, Holtzman MJ, Pierce RA. Increased iron sequestration in alveolar macrophages in chronic obstructive pulmonary disease. *PLoS One* 2014; 9: e96285.

19. Sangiuolo F, Puxeddu E, Pezzuto G, Cavalli F, Longo G, Comandini A, Di Pierro D, Pallante M, Sergiacomi G, Simonetti G, Zompatori M, Orlandi A, Magrini A, Amicosante M, Mariani F, Losi M, Fraboni D, Bisetti A, Saltini C. HFE gene variants and iron-induced oxygen radical generation in idiopathic pulmonary fibrosis. *Eur Respir J* 2015; 45: 483-490.

20. Thompson AB, Bohling T, Heires A, Linder J, Rennard SI. Lower respiratory tract iron burden is increased in association with cigarette smoking. *J Lab Clin Med* 1991; 117: 493-499.

21. Eldem I, Ileri T, Ince E, Asarcikli F, Pekpak E, Cakmakli HF, Ceyhan K, Uysal Z. Idiopathic Pulmonary Hemosiderosis With Allergic Asthma Diagnosis in a Pediatric Patient. *J Pediatr Hematol Oncol* 2015; 37: e435-437.

22. Wang J, Pantopoulos K. Regulation of cellular iron metabolism. *Biochem J* 2011; 434: 365-381.

23. Smit JJ, van Loveren H, Hoekstra MO, Nijkamp FP, Bloksma N. Influence of the macrophage bacterial resistance gene, Nramp1 (Slc11a1), on the induction of allergic asthma in the mouse. *FASEB J* 2003; 17: 958-960.

24. Ali MK, Kim RY, Karim R, Mayall JR, Martin KL, Shahandeh A, Abbasian F, Starkey MR, Loustaud-Ratti V, Johnstone D, Milward EA, Hansbro PM, Horvat JC. Role of iron in the pathogenesis of respiratory disease. *Int J Biochem Cell Biol* 2017; 88: 181-195.

25. Giorgi G, D'Anna MC, Roque ME. Iron homeostasis and its disruption in mouse lung in iron deficiency and overload. *Exp Physiol* 2015; 100: 1199-1216.

26. Fan Y, Zhang J, Cai L, Wang S, Liu C, Zhang Y, You L, Fu Y, Shi Z, Yin Z, Luo L, Chang Y, Duan X. The effect of anti-inflammatory properties of ferritin light chain on lipopolysaccharide-induced inflammatory response in murine macrophages. *Biochim Biophys Acta* 2014; 1843: 2775-2783.

27. Ramakrishnan K, Borade A. Anemia as a risk factor for childhood asthma. *Lung India* 2010; 27: 51-53.

28. Vlasic Z, Dodig S, Cepelak I, Topic RZ, Zivcic J, Nogalo B, Turkalj M. Iron and ferritin concentrations in exhaled breath condensate of children with asthma. *J Asthma* 2009; 46: 81-85.

29. Brigham EP, McCormack MC, Takemoto CM, Matsui EC. Iron status is associated with asthma and lung function in US women. *PLoS One* 2015; 10: e0117545.

30. Ekmekci OB, Donma O, Sardogan E, Yildirim N, Uysal O, Demirel H, Demir T. Iron, nitric oxide, and myeloperoxidase in asthmatic patients. *Biochemistry (Mosc)* 2004; 69: 462-467.

31. Kocyigit A, Armutcu F, Gurel A, Ermis B. Alterations in plasma essential trace elements selenium, manganese, zinc, copper, and iron concentrations and the possible role of these elements on oxidative status in patients with childhood asthma. *Biol Trace Elem Res* 2004; 97: 31-41.

32. Narula MK, Ahuja GK, Whig J, Narang AP, Soni RK. Status of lipid peroxidation and plasma iron level in bronchial asthmatic patients. *Indian J Physiol Pharmacol* 2007; 51: 289-292.

33. Altamura S, Muckenthaler MU. Iron toxicity in diseases of aging: Alzheimer's disease, Parkinson's disease and atherosclerosis. *J Alzheimers Dis* 2009; 16: 879-895.

34. Ruprai RK. Plasma oxidant-antioxidants status in asthma and its correlation with pulmonary function tests. *Indian J Physiol Pharmacol* 2011; 55: 281-287.

35. Sagdic A, Sener O, Bulucu F, Karadurmus N, Ozel HE, Yamanel L, Tasci C, Naharci I, Ocal R, Aydin A. Oxidative stress status and plasma trace elements in patients with asthma or allergic rhinitis. *Allergol Immunopathol (Madr)* 2011; 39: 200-205.

36. Iyer D, Mishra N, Agrawal A. Mitochondrial Function in Allergic Disease. *Curr Allergy Asthma Rep* 2017; 17: 29.

37. Calhoun WJ, Reed HE, Moest DR, Stevens CA. Enhanced superoxide production by alveolar macrophages and air-space cells, airway inflammation, and alveolar macrophage density changes after segmental antigen bronchoprovocation in allergic subjects. *Am Rev Respir Dis* 1992; 145: 317-325.

38. Comhair SA, Xu W, Ghosh S, Thunnissen FB, Almasan A, Calhoun WJ, Janocha AJ, Zheng L, Hazen SL, Erzurum SC. Superoxide dismutase inactivation in pathophysiology of asthmatic airway remodeling and reactivity. *Am J Pathol* 2005; 166: 663-674.

39. Smith LJ, Shamsuddin M, Sporn PH, Denenberg M, Anderson J. Reduced superoxide dismutase in lung cells of patients with asthma. *Free Radic Biol Med* 1997; 22: 1301-1307.

40. Jesenak M, Zelieskova M, Babusikova E. Oxidative Stress and Bronchial Asthma in Children-Causes or Consequences? *Front Pediatr* 2017; 5: 162.

41. Nadeem A, Siddiqui N, Alharbi NO, Alharbi MM. Airway and systemic oxidant-antioxidant dysregulation in asthma: a possible scenario of oxidants spill over from lung into blood. *Pulm Pharmacol Ther* 2014; 29: 31-40.

42. Andreadis AA, Hazen SL, Comhair SA, Erzurum SC. Oxidative and nitrosative events in asthma. *Free Radic Biol Med* 2003; 35: 213-225.

43. Ben Anes A, Ben Nasr H, Fetoui H, Bchir S, Chahdoura H, Yacoub S, Garrouch A, Benzarti M, Tabka Z, Chahed K. Alteration in systemic markers of oxidative and antioxidative status in Tunisian patients with asthma: relationships with clinical severity and airflow limitation. *J Asthma* 2016; 53: 227-237.

44. Sugiura H, Ichinose M. Oxidative and nitrative stress in bronchial asthma. *Antioxid Redox Signal* 2008; 10: 785-797.

45. Toblli JE, Cao G, Giani JF, Dominici FP, Angerosa M. Markers of oxidative/nitrosative stress and inflammation in lung tissue of rats exposed to different intravenous iron compounds. *Drug Des Devel Ther* 2017; 11: 2251-2263.

46. Friedmann Angeli JP, Schneider M, Proneth B, Tyurina YY, Tyurin VA, Hammond VJ, Herbach N, Aichler M, Walch A, Eggenhofer E, Basavarajappa D, Radmark O, Kobayashi S, Seibt T, Beck H, Neff F, Esposito I, Wanke R, Forster H, Yefremova O, Heinrichmeyer M, Bornkamm GW, Geissler EK, Thomas SB, Stockwell BR, O'Donnell VB, Kagan VE, Schick JA, Conrad M. Inactivation of the ferroptosis regulator Gpx4 triggers acute renal failure in mice. *Nat Cell Biol* 2014; 16: 1180-1191.

47. Linkermann A, Skouta R, Himmerkus N, Mulay SR, Dewitz C, De Zen F, Prokai A, Zuchtriegel G, Krombach F, Welz PS, Weinlich R, Vanden Berghe T, Vandenabeele P, Pasparakis M, Bleich M, Weinberg JM, Reichel CA, Brasen JH, Kunzendorf U, Anders HJ, Stockwell BR, Green DR, Krautwald S. Synchronized renal tubular cell death involves ferroptosis. *Proc Natl Acad Sci U S A* 2014; 111: 16836-16841.

48. Martin-Sanchez D, Ruiz-Andres O, Poveda J, Carrasco S, Cannata-Ortiz P, Sanchez-Nino MD, Ruiz Ortega M, Egido J, Linkermann A, Ortiz A, Sanz AB. Ferroptosis, but Not Necroptosis, Is Important in Nephrotoxic Folic Acid-Induced AKI. *J Am Soc Nephrol* 2017; 28: 218-229.

49. Wang H, An P, Xie E, Wu Q, Fang X, Gao H, Zhang Z, Li Y, Wang X, Zhang J, Li G, Yang L, Liu W, Min J, Wang F. Characterization of ferroptosis in murine models of hemochromatosis. *Hepatology* 2017; 66: 449-465.

50. Alvarez SW, Sviderskiy VO, Terzi EM, Papagiannakopoulos T, Moreira AL, Adams S, Sabatini DM, Birsoy K, Possemato R. NFS1 undergoes positive selection in lung tumours and protects cells from ferroptosis. *Nature* 2017; 551: 639-643.

51. Liu B, Zhao C, Li H, Chen X, Ding Y, Xu S. Puerarin protects against heart failure induced by pressure overload through mitigation of ferroptosis. *Biochem Biophys Res Commun* 2018; 497: 233-240.

52. Wenzel SE, Tyurina YY, Zhao J, St Croix CM, Dar HH, Mao G, Tyurin VA, Anthonymuthu TS, Kapralov AA, Amoscato AA, Mikulska-Ruminska K, Shrivastava IH, Kenny EM, Yang Q, Rosenbaum JC, Sparvero LJ, Emlet DR, Wen X, Minami Y, Qu F, Watkins SC, Holman TR, VanDemark AP, Kellum JA, Bahar I, Bayir H, Kagan VE. PEBP1 Wardens Ferroptosis by Enabling Lipoxygenase Generation of Lipid Death Signals. *Cell* 2017; 171: 628-641 e626.

53. Zosky GR, Iosifidis T, Perks K, Ditcham WG, Devadason SG, Siah WS, Devine B, Maley F, Cook A. The concentration of iron in real-world geogenic PM(1)(0) is associated with increased inflammation and deficits in lung function in mice. *PLoS One* 2014; 9: e90609.

Supplementary figure legends

Figure E1. Iron diets and HDM-induced experimental asthma protocol.

Figure E2. House dust mite (HDM)-induced experimental asthma. Six-8-week-old wild-type (WT) BALB/c mice were intranasally administered HDM antigen for 5 days per week for 6 weeks and then major features of experimental asthma were assessed. Total and differential immune cells were enumerated in bronchoalveolar lavage and cytospin slides stained with May-Grunwald-Giemsa (A). Tissue eosinophil numbers were assessed in chrome salt fixation-stained lung sections (B). Mucus secreting cells (MSCs) were enumerated around inflamed airways in PAS-stained lung sections (C, D). Area of collagen deposition surrounding the basement membrane of small airways was quantified in Sirius red-stained lung tissue sections, in 6-8 airways/mouse, using *ImageJ* (E). Airway hyper-responsiveness (AHR) was measured in terms of central airway resistance (Rn) to inhaled increasing concentrations of nebulised methacholine (Mch) using Flexivent apparatus (F). Scale bar: 50 μm. Data are presented as mean ± SEM (*n*=6-8), pooled from two repeat experiments. **p<0.01; ***p<0.001; ****p<0.0001 compared to PBS controls.

Figure E3. Bronchoalveolar lavage (BAL) cell profiles in house dust mite (HDM)-induced experimental asthma in WT and *Hfe*^{-/-} AKR mice. HDM was administered to ~36 week-old wild-type (WT) and *Hfe*^{-/-} AKR mice for 5 days per week for 6 weeks and then differential immune cells were enumerated in BAL and cytospin slides stained with May-Grunwald-Giemsa. Data are presented as mean ± SEM (*n*=6-10), pooled from 2 repeat experiments. *p<0.05; **p<0.01; ***p<0.001.

Supplementary tables

Table E1. Custom-designed primers for human mRNA used in qPCR analyses.

Table E2. Custom-designed primers for mouse mRNA used in qPCR analyses.

Table E3. Antibodies used for flow cytometry

Table E4. Antigenic definitions for macrophage analyses conducted by flow cytometry

Table E5. Human bronchial airway epithelial cells (pBECs) donor characteristics

Table E6. Human airway smooth muscle cell and lung fibroblast donor characteristics
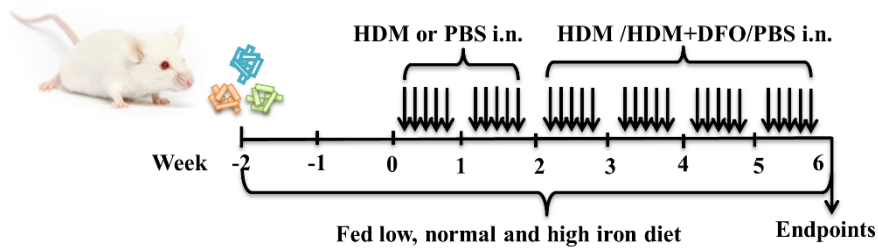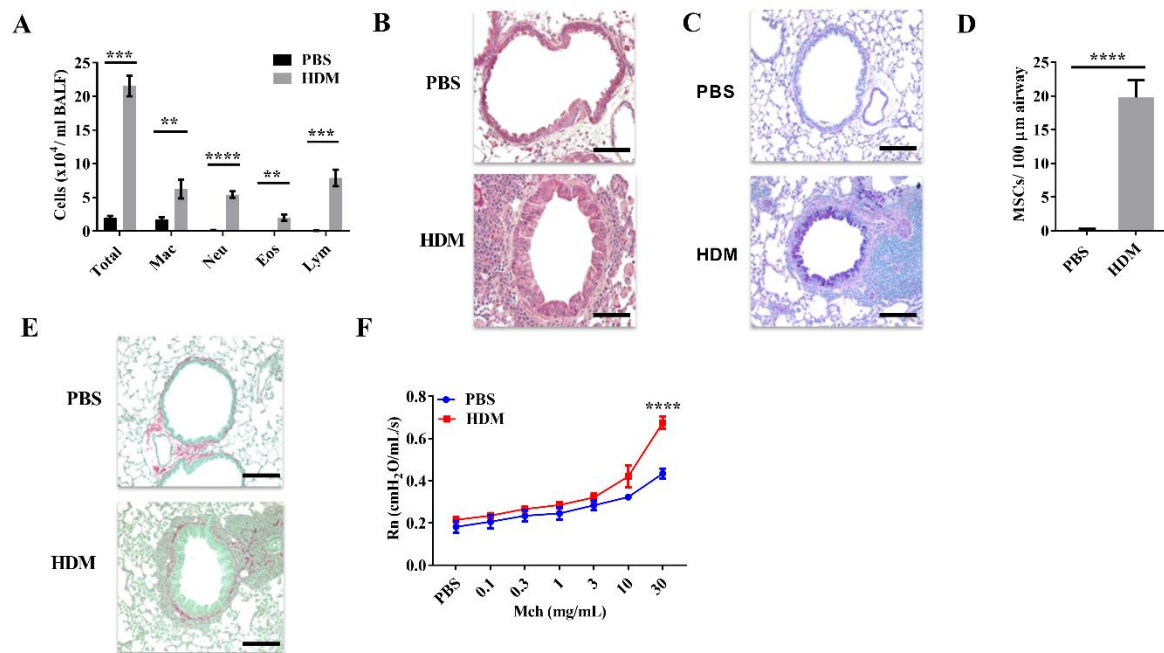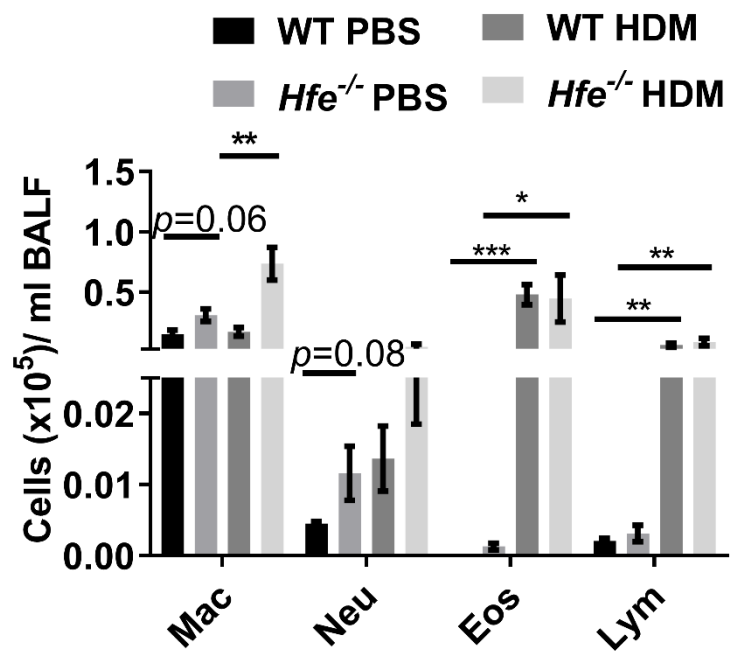
Figure E1.

Figure E2.

Figure E3.

Table E1.

Primer	Primer sequence (5' → 3')	Target gene
Beta Actin Forward	CTGGCACCACACCTTCTA	*Beta Actin*
Beta Actin Reverse	GGTGGTGAAGCTGTAGCC	*Beta Actin*
DMT1 Forward	GGT GTT GTG CTG GGA TGT TA	*DMT1*
DMT1 Reverse	AGTACATATTGATGGAACAG	*DMT1*
FPN Forward	CTGTGCCCATAATCTCTGTC	*FPN*
FPN Reverse	CCATTTATAATGCCTCTTTCAG	*FPN*
HAMP Forward	CTGTTTTCCCACAACAGACG	*HEPC1*
HAMP Reverse	CAGCACATCCCACACTTTGA	*HEPC1*
TFR1 Forward	AGGAACCGAGTCTCCAGTGA	*TFR1*
TFR1 Reverse	ATCAACTATGATCACCGAGT	*TFR1*
TFR2 Forward	GGAGTGGCTAGAAGGCTACCTCA	*TFR2*
TFR2 Reverse	GGTCTTGGCATGAAACTTGTCA	*TFR2*
FTL Forward	CCATGAGCTCCCAGATTCGT	*Ft L*
FTL Reverse	TTCCAGAGCCACATCATCGC	*Ft L*
FTH Forward	CCAGAACTACCACCAGGACT	*Ft H*
FTH Reverse	CACATCATCGCGGTCAAAGT	*Ft H*
ZIP14 Forward	GCTTATGGAGAACCACCCCT	*ZIP14*
ZIP14 Reverse	AGGTTCCTGTGTCCTTGCAC	*ZIP14*
NRAMP1 Forward	TTCTCGTCCAAAGGAGCAGG	*NRAMP1*
NRAMP1 Reverse	GTTGCAGGCGGAACAGAAAG	*NRAMP1*
IRP1 Forward	CGTGCAGTCGGAGGAACAC	*IRP1*
IRP1 Reverse	TCGAAAATGGTAAGCGCCCA	*IRP1*

Table E2.

Primer	Primer sequence (5' → 3')	Target gene
Hprt Forward	AGGCCAGACTTTGTTGGATTTGAA	*Hprt*
Hprt Reverse	CAACTTGCGCTCATCTTAGGCTTT	*Hprt*
Il13 Forward	TGCTTGCCTTGGTGGTCT	*Il13*
Il13 Reverse	GGGGAGTCTGGTCTTGTGTG	*Il13*
Tfr1 Forward	CCCATGACGTTGAATTGAACCT	*Tfr1*
Tfr1 Reverse	GTAGTCTCCACGAGCGGAATA	*Tfr1*
Il10 Forward	AGGCGCTGTCATCGATTTCT	*Il10*
Il10 Reverse	ATGGCCTTGTAGACACCTTGG	*Il10*
Ifng Forward	CTGGAGGAACTGGCAAAAGG	*Ifng*
Ifng Reverse	TTGCTGATGGCCTGATTGTC	*Ifng*
Tgfb1 Forward	CCCGAAGCGGACTACTATGCTA	*Tgfb1*
Tgfb1 Reverse	GGTAACGCCAGGAATTGTTGCTAT	*Tgfb1*

Table E3. Antibodies used for flow cytometric staining

Antigen	Fluorophore	Clone	Manufacturer
CD45	PerCP	30F-11	Biolegend
CD11c	Brilliant violet (BV)421	N418	Biolegend
CD11b	Alexa Fluor (AF)700	M1/70	BD Biosciences
SiglecF	Phycoerythrin (PE)	E50-2440	BD Biosciences
F4/80	BV711	T45-2342	Biolegend
Ly6C	PE-Cy7	A1-21	BD Biosciences
TFR1	APC	R17217	Biolegend

Table E4. Antigen definitions for macrophage flow cytometric staining

Granulocyte type	Antigen definition
Total macrophages	$CD45^+$, $F480^+$, $CD11c^{hi/+/-}$, $SiglecF^{-/hi}$
Alveolar Macrophage	$CD45^+$, $F4/80^+$, $CD11b^-$, $CD11c^{hi}$ $SiglecF^{hi}$
Interstitial Macrophage	$CD45^+$, $F4/80^+$, $CD11b^+$, $CD11c^+$, $SiglecF^-$, $Ly6C^-$
Monocytes	$CD45^+$, $F4/80^+$, $CD11b^+$, $CD11c^-$, $SiglecF^-$, $Ly6C^+$

Table E5.

Characteristic	Healthy	Asthmatics
Number of subjects, n	8	7
Age, yr	62.63 ± 5.873	56.86 ± 5.595
Sex, M/F	2/6	2/5
FEV1% predicted	84.25 ± 5.230	78.43 ± 6.931
FEV1/FVC	0.747 ± 0.030	0.723 ± 0.021
ACQ	-	2.400 ± 0.623
Total cells (x10^6/mL BAL)	0.667 ± 0.391	3.717 ± 3.345
Macrophages (%)	47.75 ± 13.93	41.67 ± 13.48
Neutrophils (%)	22.75 ± 11.00	44.29 ± 14.64
Eosinophils (%)	0.850 ± 0.217	1.833 ± 0.363
ICS, yes/no	NA	7/0
ICS dose$^\$$	NA	717.10 ± 114.7
LABA, yes/no	NA	6/1
LAMA, yes/no	NA	2/5
SABA, yes/no	NA	3/4
OCS, yes/no	NA	0/7

M/F, male/female; FEV1, forced expiratory volume in one second; FVC, forced vital capacity; ACQ, asthma control questionnaire; BAL, bronchoalveolar lavage; NA, not applicable; ICS, inhaled corticosteroids; LABA, long-acting β2-agonist; LAMA, long-acting muscarinic antagonist; SABA, short-acting β-agonist; OCS, oral corticosteroids; yr, year. $^\$$Equivalent to Fluticasone μg/day. Data are shown as mean ± SEM.

Table E6.

Patient No.	Disease	Gender	Age
1	Pulmonary fibrosis	F	54
2	Pulmonary fibrosis	M	64
3	Bronchiectasis	M	60
4	IPF	M	65
5	Telomere-associated pulmonary fibrosis	F	45
6	COPD	M	61
7	NSCC	F	60
8	Pulmonary fibrosis	M	68
9	Emphysema	F	57
10	Emphysema	M	65
11	bronchiectasis	F	38
12	BOS (re-do)	F	28

| 13 | Emphysema | M | 60 |
| 14 | Pulmonary fibrosis | M | 53 |

M, male; F, female.